Pharm Res (2012) 29:236–250
DOI 10.1007/s11095-011-0538-y

RESEARCH PAPER

Distinct Aggregation Mechanisms of Monoclonal Antibody Under Thermal and Freeze-Thaw Stresses Revealed by Hydrogen Exchange

Aming Zhang • Satish K. Singh • Michael R. Shirts • Sandeep Kumar • Erik J. Fernandez

Received: 13 May 2011 / Accepted: 7 July 2011 / Published online: 30 July 2011

ABSTRACT

Purpose Aggregation of monoclonal antibodies (mAbs) is a common yet poorly understood issue in therapeutic development. There remains a need for high-resolution structural information about conformational changes and intermolecular contacts during antibody aggregation.

Methods We used hydrogen exchange mass spectrometry (HX-MS) to compare the aggregation mechanism and resultant aggregate structures of the pharmaceutical antibody Bevacizumab under freeze-thaw (F/T) and thermal stresses.

Results Bevacizumab aggregation increased with number of F/T cycles and decreased with protein concentration. HX-MS showed native-like aggregates. Conversely, thermal stress triggered non-native aggregation at temperatures below melting point of the least stable CH2 domain. Under these conditions, HX was significantly enhanced in much of the Fab fragment while being decreased relative to native HX in CDRs. Analysis of intrinsic fluorescence Trp and extrinsic ANS dye binding supported structural differences between two antibody aggregates formed by F/T *vs*. thermal stresses.

Conclusions Reduced hydrogen exchange in three CDRs suggests these residues may form strong intermolecular contacts in the antibody aggregates; regions of enhanced HX indicate unfolding. Residue level modeling methods with varying levels of atomistic detail were unable to identify aggregation patterns predictively.

KEY WORDS aggregation · freeze-thaw · hydrogen exchange · monoclonal antibody · structure

ABBREVIATIONS

ACN	acetonitrile
ANS	anilino-8-naphthalene sulfonate
D_2O	deuterium oxide
F/T	freeze-thaw
HC	heavy chain
HPSEC	high performance size exclusion chromatography
HX	hydrogen exchange
LC	light chain
mAbs	monoclonal antibodies
MS	mass spectroscopy
SAP	spatial aggregation propensity
TCEP	*tris*(2-carboxyethyl)phosphine

INTRODUCTION

Monoclonal antibodies (mAbs) constitute a major class of therapeutic proteins because of their definitive mechanisms of action and high specificity (1). They are expected to grow in popularity for the foreseeable future, as hundreds of mAbs candidates are in different stages of preclinical or clinical

Electronic Supplementary Material The online version of this article (doi:10.1007/s11095-011-0538-y) contains supplementary material, which is available to authorized users.

A. Zhang • M. R. Shirts • E. J. Fernandez (✉)
Department of Chemical Engineering, University of Virginia
102 Engineers' Way
Charlottesville, Virginia 22904-4741, USA
e-mail: erik@virginia.edu

S. K. Singh • S. Kumar
Pfizer Inc., BioTherapeutics Pharmaceutical Sciences
Chesterfield, Missouri 63017, USA

Present Address:
A. Zhang
Formulation and Analytical Resource, Amgen
Thousand Oaks, California 91320, USA

development. Although mAbs are generally quite thermodynamically stable relative to other protein therapeutics, they also tend to degrade by different pathways, either chemically or physically, when exposed to a wide variety of external stresses (2), particularly in high concentration formulations required for most mAb therapeutic products (3). Therefore, a major ongoing challenge for developing safe and potent mAb therapeutics is to design rational manufacturing processes and final dosage formulations that can prevent or minimize antibody degradation and ensure product quality within the required shelf life (1,3).

Among the various degradation pathways, aggregation of mAbs into high molecular weight species has been an increasing concern in therapeutic development, partially because protein aggregates are generally believed to be a potential cause of side effects and enhanced immunogenic responses observed in clinical trials (4,5). Therefore, it is of great significance to understand the aggregation mechanism of mAbs exposed to different processing stresses as well as the relationship between various types of mAb aggregates and their potential biological implications in the pharmaceutical industry.

As a major class of approved therapeutic protein products and candidates, aggregation of IgG antibodies has been extensively studied (1). The highly conserved sequence and structure in the constant domains have resulted in some common features observed for IgG aggregation in the mounting literature. For instance, the CH2 domain of antibodies has been generally suggested to be more sensitive to pH change and can adopt a more flexible conformation at low pH than the native state at neutral pH (6). Consistent with this, IgG aggregation at low pH has been proposed to be triggered by CH2 domain interactions in previous studies (7). By contrast, the Fab fragment of IgG antibodies has been observed to be more susceptible to other environmental stresses, such as high temperature (7,8), agitation (7) and high concentration formulation (9). It is interesting to note that the Fab fragment generally has higher thermal stability than the CH2 domain, and yet Fab-Fab interactions have been implicated in thermally induced antibody aggregation (7,8). This may be partially because antibody unfolding and/or aggregation associated with CH2 domain are reversible when the thermal stress is removed (10).

Beyond these initial studies, there remain several open questions about antibody aggregation. For instance, a wide variety of aggregation behaviors and mechanisms have been suggested for different antibody molecules exposed to varying processing stresses in previous studies (7,8,11). However, the aggregation mechanisms of the same antibody under different stresses or aggregation conditions have not been carefully compared. Second, the molecular structure of different antibody aggregates formed under various conditions is generally characterized only at low resolution and/or in globally averaged sense due to the lack of experimental techniques. Thus, it remains difficult to correlate aggregate types and structural features with various biological implications, such as adverse side effects and enhanced immunogenicity observed in clinical trials (12). Third, antibodies are multi-domain proteins, and the domain involved in unfolding and aggregation is challenging to identify. Previous attempts to do this have been based mainly on the comparison of aggregation kinetics between intact antibody and the isolated Fab and Fc fragments to identify the responsible domain(s) (7,10,11). Evidence from direct analysis of antibody aggregates is scarce. In a few studies, molecular structure changes associated with the aggregation process were monitored by CD, FTIR and/or fluorescence (8); however, these spectroscopic techniques have insufficient resolution to reveal the regions or domain(s) involved in conformational changes during antibody aggregation.

In this study, we compare the distinct aggregation mechanisms of one antibody molecule under two common processing stresses: freeze-thaw (F/T) processing and high temperature. Freeze-thaw combines a number of stressing factors that can potentially cause protein denaturation and/or aggregation. These factors include cold denaturation (13), generation of ice-solution interface (14), solute crystallization (15) and pH shift (16). To date, determination of the primary stress responsible for the observed protein damage remains a challenge for rational F/T process development. In contrast, high temperature usually leads to sequential unfolding of individual domains in antibody structure, and the accumulation of these partially unfolded intermediates can trigger self-association (7,9). As a consequence, thermally induced antibody aggregation usually involves conformational changes (8). Further, the Fab fragment has been indicated to play a critical role for antibody aggregation under thermal stress (7,8). However, to our knowledge, there are no studies identifying the intermolecular contacts in the formed aggregates.

Hydrogen/deuterium exchange detected by mass spectrometry (HX-MS) is a useful technique to characterize protein structure in both monomeric and aggregate state (17). In combination with proteolytic fragmentation, this technique also enables peptide level structure analysis for protein monomers comprising the aggregates (17,18). In this study, we investigate the structures and aggregation mechanism of the pharmaceutical antibody Bevacizumab (marketed as Avastin®) under freeze-thaw and thermal stresses using HX-MS. Our results suggest that Bevacizumab aggregates formed after a number of F/T cycles are made up of monomers with native like structure. In contrast, under thermal stress, significant disordering was demonstrated by considerably increased HX in the Fab

fragment during aggregation. Notably, increases in solvent protection relative to the native monomer were also observed, perhaps identifying the regions involved in intermolecular contacts in the aggregates.

MATERIALS AND METHODS

Materials

The pharmaceutical monoclonal antibody Bevacizumab (Avastin®) was produced by Genentech and is commercially available. Deuterium oxide (D_2O) was obtained from Cambridge Isotope Laboratories (99.9% Deuterium, Andover, MA). Trehalose and 1-anilino-8-naphthalene sulfonate (ANS) were obtained from Sigma. All other reagents were HPLC purity grade and purchased from Sigma unless otherwise specified.

Bevacizumab Sample Preparation

Monoclonal antibody Bevacizumab was purchased in 25 mg/ml stock solution containing 51 mM sodium phosphate, 60 mg/ml a,a-trehalose dehydrate and 0.04% polysorbate 20, pH 6.2. This is significantly lower than the previously reported pI (8.4–8.5) (19) of the molecule. To conduct aggregation studies in the absence of stabilizing excipients and surfactant, a buffer exchange step was performed using Protein A chromatography. Briefly, 1 ml formulated Bevacizumab solution was diluted into 25 ml PBS buffer (pH 6.2) and loaded onto a pre-equilibrated Protein A column (1 ml, GE Healthcare). Bevacizumab was eluted in 0.1 M citric buffer pH 3.0 and collected in multiple 1.5 centrifuge tubes. The collected Bevacizumab fractions were pooled and then dialyzed three times against 20 mM citric buffer containing 100 mM NaCl, pH 6.2. The dialyzed Bevacizumab solution was centrifuged at 15,000 g for 20 min to remove possible preformed aggregates. Following centrifugation, Bevacizumab supernatant was stored at 4°C until use. Bevacizumab concentration was determined by measuring A_{280} absorbance using an extinction coefficient of 1.661 mL/mg-cm calculated by the ExPASy Proteomics Server ProtParam (http://expasy.org/tools/protparam.html).

Freeze-Thaw and Thermal Treatments

In F/T-induced aggregation, buffer-exchanged Bevacizumab solution was diluted appropriately to make desired protein concentrations at 0.50, 1.00 and 2.50 mg/ml in 20 mM citric buffer, pH 6.2. The resultant Bevacizumab samples (400 μL in centrifuge tubes) were frozen in liquid N_2 for 5 min followed by thawing in 25°C water bath for 5 min. Up to 30 F/T cycles were applied to produce extensive aggregation. For thermally induced aggregation, 400 uL Bevacizumab samples (0.5 mg/ml after dilution) were incubated at 65 and 70°C in a recirculating water bath for different periods of time. Aggregation was quenched by incubating samples in an ice bath for 3 min.

High Performance Size Exclusion Chromatography (HPSEC)

HPSEC was performed on a BioLogic DuoFlow chromatography system (BioRad, Hercules, CA) at room temperature. Before being loaded to the SEC column, all the aggregate samples were centrifuged at 15,000 g for 20 min to remove large, insoluble aggregates. In each run, 150 μL supernatants were applied to a pre-equilibrated TSKgel SEC column (G3000 SWXL, 7.8 mm×30 cm, Tosoh Bioscience, Bellefonte, PA). Bevacizumab was then eluted with 0.3 M NaCl, 50 mM PBS (pH 7.0). The mobile phase flow rate was 1 mL/min. For each sample, at least two replicates were performed. The aggregation was qualitatively estimated by the loss of monomer peak after normalization to the peak area of an untreated Bevacizumab sample at the same protein concentration.

Trp Fluorescence Measurement

Trp fluorescence measurements of native Bevacizumab monomer and aggregate samples after F/T and thermal treatment were performed at room temperature on a FluoroMax-3 spectrofluorometer (Horiba Jobin Yvon, Edison, NJ). A quartz cell with 5 mm path length (Part number 4ES5X5, Precision Cells Inc., Farmingdale, NY) was used. In the measurement, 80 μL Bevacizumab samples (0.5 mg/ml) were diluted 5-fold in 20 mM citric buffer. The samples were excited at 295 nm, and the emission spectrum was recorded over a wavelength range of 300–450 nm. Three scans were performed to obtain an average spectrum for each sample.

ANS Binding Analysis

Fluorescence spectra of ANS binding to native or aggregated Bevacizumab samples were obtained at room temperature on a FluoroMax-3 spectrofluorometer (Horiba Jobin Yvon, Edison, NJ). A quartz cell with 5 mm path length (Part number 4ES5X5 Precision Cells Inc., Farmingdale, NY) was used. In each measurement, 80 uL Bevacizumab samples (0.5 mg/ml) were diluted 5-fold with 20 mM citric buffer (pH 6.2) and then mixed with 40 μL of 2 mM ANS stock solution. Samples were excited at 390 nm, and the emission spectrum was recorded over a wavelength range of 410–600 nm. All the measurements

were carried out within 5 min of sample mixing, and three scans were performed to obtain an average spectrum for each sample.

HX Analysis of Bevacizumab Structure in the Frozen State

Antibody structure in the frozen state was analyzed using the same protocol as described in our previous study for model protein lactate dehydrogenase (Zhang A. *et al.* Pharm Res, in press). Briefly, Bevacizumab stock solution was diluted in H_2O-based citrate buffer (20 mM sodium citrate, 100 mM NaCl, pH 6.2) to make desired protein concentrations. The sample was then mixed at 1:9 volume ratio with D_2O-based citrate buffer (the same solution composition and pH 6.2 as read). The resultant Bevacizumab solution had 90% deuterium in the solvent and protein concentrations of 0.02, 0.05 and 0.10 mg/ml. To minimize H/D exchange in the solution phase before sample freezing, the mixing of Bevacizumab solution and D_2O-based buffer was carried out in the shortest time possible for manual operation (less than 2 s), immediately followed by flash freezing in liquid N_2 for 5 min. Frozen Bevacizumab samples were then transferred to a −10°C freezer to allow H/D exchange for 24 h. Thawing of the deuterium-labeled frozen sample was achieved by adding twice the sample volume of 50 mM citrate buffer (pH 2.5, ice cold) containing 6 M Guanidine HCl. Back exchange was minimized by lowering the pH to ~2.8 during the thawing period. Further, the time for complete thawing of the frozen sample was reduced to 2 min by the high concentration of Guanidine HCl.

HX Analysis of Native Bevacizumab and Two Stress-Induced Aggregates in Solution

HX structure analysis of Bevacizumab aggregates formed after F/T and thermal treatments were carried out in the solution state. One hundred μL F/T- or thermal-treated samples were centrifuged at 15,000 g for 15 min to pellet aggregates, and 90 μL supernatant was carefully removed. HX was initiated by adding 90 μL D_2O into the aggregate pellets. HX in solution was carried out at room temperature for durations of 0.17, 1, 10, 60 and 180 min, and then arrested by adding ice-cold quenching buffer (50 mM citrate buffer containing 6 M Guanidine HCl and 0.5 M *tris*(2-carboxyethyl)phosphine (TCEP), pH 2.5). In this protocol, 6 M Guanidine HCl was effective for dissociating Bevacizumab aggregates back into fully unfolded monomers, while 0.5 M TCEP reduced antibody disulfide bonds to facilitate subsequent online digestion using immobilized pepsin.

For LC-MS analysis, quenched Bevacizumab sample was diluted 5-fold into 0.1% formic acid (pH 2.5) before loading into the sample loop. Proteolytic fragmentation of antibody was achieved by flowing the sample through an on-line immobilized pepsin column. The resulting peptide mixture was desalted on a peptide-trapping column (1 mm ID×8 mm, catalog No. TR1/25108/01; Michrom Bioresources, Auburn, CA) for 6 min and then separated in a second peptide-resolving column (Kinetex 2.6 μm C_{18}, 2.10×100 mm, Phenomenex, Torrance, CA). For good peptide separation, a shallow ACN elution gradient (from 15 to 40% over 20 min) was used for the resolving column. All the reporter peptides used for HX analysis were assigned by performing tandem (MS/MS) mass spectrometry, followed by analysis with TurboSEQUEST software. To minimize artifactual isotope exchange during the analysis time, all the columns, loops, and lines were immersed in an ice bath during all the experiments.

The deuteration level for each reporter peptide was calculated by the following equation:

$$D\% = \frac{m - m_0}{(m_{100} - m_0)} \times 100\% \quad (1)$$

where m is the measured centroid mass of the deuterated molecule or peptide after a particular labeling time, and m_0 and m_{100} are the two centroid mass limits of a molecule and reporter peptide from zero-deuteration and full-deuteration control experiments, respectively.

Spatial Aggregation Propensity (SAP) Calculation

The starting structures for simulations for Bevacizumab were generated by MOE (Chemical Computing Group, version 2008.1), modeled from antibody PDB structures 1HZH and 1IGY, with 1334 total residues and 20336 atoms for each of the two structures. No glycosylation was introduced. All simulations were performed using the Python interface pyopenmm (http://www.simtk.org/home/pyopenmm) to the GPU simulation code OpenMM (http://www.simtk.org/home/openmm) (20) on the NCSA Lincoln GPU cluster. Four simulations were performed. Two simulations were started from each of the two modeled pdb structures using different random number seeds for velocities. The proteins were simulated with AMBER ff99sb force field (21) with the Onufriev-Bashford-Case generalized Born/surface area implicit solvent model (22) with no cut-offs. Numerical integration was performed with Langevin dynamics with a collision rate of parameter of 5 ps^{-1} and a 2 fs time step with hydrogen atoms constrained by SHAKE (23). Temperature was maintained by the Langevin dynamics at 298 K.

Structures were minimized using L-BFGS minimization, with less than 1Å deviation from the modeled structure, and a total of 15 ns of simulation was performed for each structure, with the first 1 ns discarded as equilibration.

Structures were collected every 5 ps, and all averages are over the 2800 structures collected during the last 14 ns of the simulation. Because of the use of GPU accelerated code, simulation data were collected at a rate of 5.0 ns/day for each simulation, meaning these simulations are not particularly constrained by the wall clock time required.

Spatial aggregation propensity is defined as described previously (24,25), though we express it mathematically in a slightly different form here for clarity. SAP is a function of some user-specified cut-off distance R and is defined for each atom i of the structure as

$$SAP(R,i) = \frac{1}{N_{\text{structures}}} \sum_{\text{All structures}} \left\{ \sum_{\substack{\text{Side chain atoms j} \\ \text{with distance } r_{ij} < R}} SAA_j \times \left(\frac{H_j}{TSAA_j} \right) \right\} \tag{2}$$

where r_{ij} is the distance between atoms i and j, SAA_j is the solvent accessible surface area of atom j, H_j is the normalized hydrophobicity of the type of residue atom j belongs to (see Table S1), and $TSAA_j$ is the total maximum solvent accessible surface area of the type of residue atom j belongs to (see Table S1 for parameters).

For the current study, surface area was determined per heavy atom using default parameters of POPSc (26). Since the surface area calculation was performed using heavy atoms instead of all atoms, the sum over all side chain atoms in Eq. 2 was replaced with a sum over all side chain heavy atoms, and SAP was calculated for only the heavy atoms. Because the calculation used heavy atoms, we recalculated the maximum surface area per side chain instead of using the tabulated numbers from previous studies (24,25). Maximum surface area per side chain was determined by building each amino acid trimer Ala-X-Ala in Pymol (commercialized version of 1.12r1) in an extended conformation. If the first side chain dihedral angle, χ_1, defined by N-Cα-Cα-Cγ, was not present in the side chain, the maximum surface area of the side chain was calculated from this extended structure. If χ_1 was present, then the maximum surface area was calculated by rotating χ_1 by 1 ° intervals and choosing maximum surface area of the side chain atoms generated over the entire 360-degree rotation. As in previous studies, a cut-off of 5Å was used for identifying potential aggregation sites (24,25). SAP is a statistical quantity, and our analysis reveals that SAP appears to be statistically accurate enough to identify regions that have high SAP independent of the simulation starting conditions. We can check the consistency of the SAP calculation as a function of separate simulations by comparing sets of data that should give identical SAP values in the infinitely long simulation limit. For example, in the infinite limit, SAP for the same sequence with two different templates, two chains related by symmetry, and runs with the same structure and different random number seeds should all be the same.

For cut-off R = 5Å, we find that the average standard error in SAP of corresponding residues over all four simulations is less than 0.024 for both chains of the 1HZH template structure and 0.025 for both chains l the 1IGY template structure. The average standard error in SAP for corresponding resides over all eight runs is less than 0.027 for all chains. In previous studies, peaks in SAP greater than 0.15 are correlated with aggregation prone regions. This statistical analysis demonstrates that these different simulations should be sufficiently consistent across all runs and templates to identify regions with high SAP values. We can also compare the reliability of the data sets in terms of Pearson's correlation coefficient. The average correlation coefficient between data sets from the same template and chain, differing only by a random number seed, is 0.95. The average correlation coefficient between all pairs of residue-averaged SAPs, including symmetry-related copies from different simulations but the same template is 0.90. The average correlation coefficient between all pairs of residues from different templates is 0.83. These statistics indicate again that the trends in SAP are very consistent, though there is moderate uncertainty due to protein fluctuations.

Additionally, we also found that the correlation coefficient between our SAP values with a modified protocol and previous SAP calculations (24,25) for the conserved Fc domain is 0.82 over all models and chains, approximately the same as exists between simulations run with different templates. However, there exist some differences in the characteristics of SAP calculated, because of differences in the protein parameters, the solvent model, and the solvent accessible surface area calculation. We found that our modified protocol had a tendency to underestimate large negative (hydrophilic) SAP values compared to the previously published protocol (see Figure S1). However, most peaks matched quantitatively, and virtually all residue level trends were replicated, as must be the case because of high correlation.

RESULTS

HX Analysis of Bevacizumab Structure in the Frozen State

Trehalose is a commonly used cryoprotectant which has been shown to protect protein from freezing-induced structure denaturation previously (27). Therefore, Bevacizumab frozen in the presence of 1 M trehalose was regarded to be the most stable condition, presumably representing native antibody conformation in the frozen

state. To detect any potential structural perturbations to Bevacizumab caused by freezing, the HX pattern of Bevacizumab frozen in the absence of cryoprotectant was measured and compared to that of native control with 1 M trehalose. In Fig. 1, it can be seen that for both LC and HC, the majority of reporter peptides from two frozen Bevacizumab states with and without 1 M trehalose showed very similar deuterium labeling (as indicated by the same color for the same reporter peptide). A few reporter peptides that were mapped by different color bars between two samples were denoted by the specific values of deuterium labeling in the HX pattern for both LC and HC. These values indicated that this group of reporter peptides also had similar deuterium labeling, differing by ~10% or less. The close HX patterns measured for two frozen Bevacizumab samples with and without trehalose protection suggested that the freezing process had minor impact on the antibody structure.

The impact of freezing on Bevacizumab structure integrity was analyzed using the same HX-MS protocol in the frozen state as previously described (28). Figure 1a, b shows the peptide level HX patterns of Bevacizumab light chain (LC) and heavy chain (HC), respectively, under a variety of designed freezing conditions. From top to bottom in each panel, the analyzed samples include Bevacizumab frozen in the presence of (a) 1 M trehalose, (b) without any additives to the citrate buffer, and (c–e) with the addition of 25, 100, and 200 mM guanidine HCl, respectively. Each set of five horizontal bars under the sequence represents one corresponding reporter peptide. The color of each bar indicates the degree of hydrogen/deuterium exchange (scale shown in the right of Fig. 1a) measured after 24 h labeling in the frozen state (−10°C) in 90% D_2O-rich solvent. The numbers adjacent to horizontal bars in Fig. 1 denote the quantitative values of deuterium labeling calculated by Eq. 1 for the corresponding reporter peptides.

To further examine antibody stability against freezing stress, we increased the denaturing stress in the frozen state by adding 25 to 200 mM guanidine HCl to the initial sample solution. After freeze-induced concentration, the denaturant could reach approximately 0.25 to 2 M in the frozen state according to the estimation described before (29). The HX patterns measured for frozen Bevacizumab samples with increasing guanidine HCl concentration were also shown in Fig. 1. For the LC in Fig. 1a, it can be seen that increasing guanidine HCl from 0 to 200 mM did not result in significant changes in deuterium labeling for all the reporter peptides across the sequence. It suggested that Bevacizumab LC could maintain its native-like structure in the presence of ≤2 M guanidine HCl in the frozen state. In contrast, for the HC in Fig. 1b, reporter peptides from multiple regions showed significantly increased deuterium labeling as the guanidine HCl concentration increased up to 2 M in the frozen state. Four regions with most prominent increase in deuterium labeling (>20%) are highlighted by red ovals in Fig. 1b. These regions are located in different domains, suggesting freezing process with increasing denaturant partially denatured all the HC domains simultaneously.

F/T and Thermally Induced Bevacizumab Aggregation

Bevacizumab aggregation induced by F/T and high temperature was qualitatively analyzed by HPSEC. In F/T-induced aggregation, the effect of protein concentration and the number of F/T cycles on Bevacizumab aggregation was investigated. Figure 2a shows the degree Bevacizumab aggregation at three different protein concentrations at 0.5, 1.0 and 2.5 mg/ml after subjecting to 10 F/T cycles. The HPSEC elution profiles of three Bevacizumab samples were normalized to samples at identical protein concentrations that were not freeze-thawed. In Fig. 2a, all three aggregate samples after 10 F/T cycles showed one single peak eluting at the same retention time as native Bevacizumab, indicating the aggregates species was completely removed by centrifugation in the loaded samples. The normalized monomer peak was observed to increase with protein concentration, suggesting that F/T-induced aggregation was inversely dependent on protein concentration. The effect of F/T cycle number on antibody aggregation is shown in Fig. 2b. Here, a low protein concentration (0.5 mg/ml) was used to reduce F/T cycles to get a similar degree of Bevacizumab aggregation at high concentration. As expected, the monomer peak decreased with increasing F/T cycles. After 30 F/T cycles, there was only a small fraction of native Bevacizumab (< 30%) remaining in the sample. To prepare F/T-induced aggregates for structure analysis below, we applied 30 F/T cycles to 0.5 mg/ml Bevacizumab sample.

Thermal stability of intact Bevacizumab and its isolated Fab and Fc fragments has been carefully analyzed using DSC in a previous study (30). The study revealed two unfolding transitions for intact Bevacizumab that were attributed to the overlapped unfolding of CH2 domain (70.1°C) and Fab fragment (74.1°C) in the first major transition, and CH3 domain unfolding (80.2°C) in the second small transition. For thermally induced aggregation study here, incubation temperature of a few degrees below the unfolding point of the least stable CH2 domain was used to retain the majority of native structure during antibody aggregation. Bevacizumab concentration was the same (0.5 mg/ml) as used in F/T-induced aggregation analysis.

Bevacizumab aggregates produced by incubation at two elevated temperatures 65 and 70°C are shown in Fig. 2 c and d, respectively. In contrast to F/T-induced aggregation, one obvious difference in the SEC profiles for

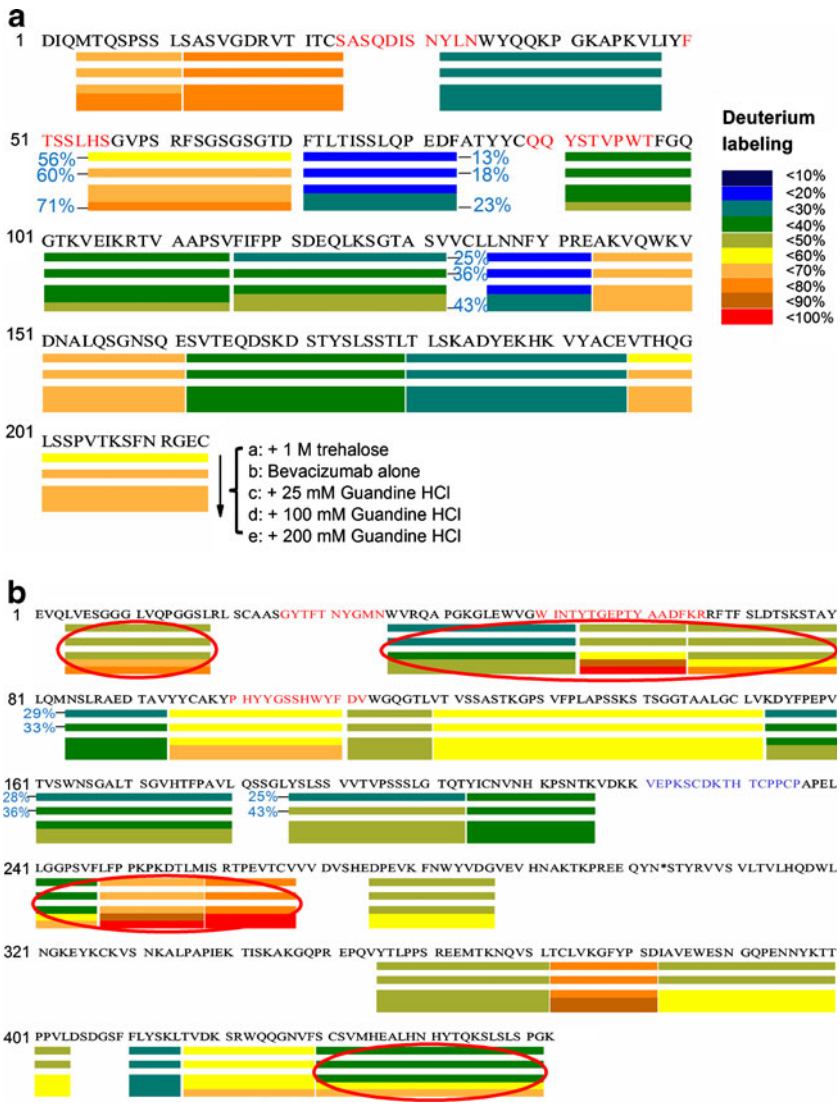

Fig. 1 Peptide level HX patterns of light chain (**a**) and heavy chain (**b**) of Bevacizumab frozen in different conditions. From top to bottom: condition, with 1 M trehalose in the sample solution; b, no additives to the sample solution; c–e, with 25, 100 and 200 mM guanidine HCl in the sample solution. Each set of five bars under the sequence shows the degree of deuterium labeling for corresponding reporter peptides with the color scale in the right of (**a**). The numbers in (**a**) denote the deuterium labeling values for neighboring reporter peptides. The red ovals indicate the regions in the HC with dramatic increase in HX after including guanidine HCl in solution.

thermally induced aggregations is the presence of an additional peak eluted before native monomer at 6–8 min. This elution peak increased at early incubation times and then decreased with further aggregation at both incubation temperatures, suggesting soluble oligomers of Bevacizumab accumulated at the intermediate time before converting to large insoluble aggregates. Aggregation kinetics at two elevated temperatures can be qualitatively compared by looking at the monomer peak loss. Clearly, higher temperature led to faster aggregation. At 70°C, almost complete aggregation was observed within 10 min, while at 65°C a similar degree of aggregation took longer than 180 min. However, the structure of Bevacizumab aggregates formed at two incubation temperatures appeared to be similar, as suggested by both Trp fluorescence and ANS binding (data not shown). Therefore, only the aggregates prepared at 70°C for 10 min were used for more detailed structure analysis using HX-MS below.

Structure Analysis of F/T-Induced Bevacizumab Aggregates by HX-MS

F/T-induced aggregates were isolated and characterized by peptide level HX as described in the Materials and Methods section. Figure 3 shows the peptide level HX patterns of both LC and HC measured *versus* labeling time for native Bevacizumab and F/T-induced aggregates. In Fig. 3, each horizontal block under Bevacizumab sequence shows the time course of deuterium labeling for one reporter peptide. Five color bars comprising the horizontal block represent the degree of deuterium labeling at labeling times of 10 s, 1, 10, 60 and 180 min (from top to bottom), respectively. For each reporter peptide, two blocks of HX are shown, comparing the local deuterium labeling between native Bevacizumab (top) and F/T-induced aggregates (bottom).

In Fig. 3a, it can be seen that native Bevacizumab and F/T-induced aggregates exhibited very similar deuterium

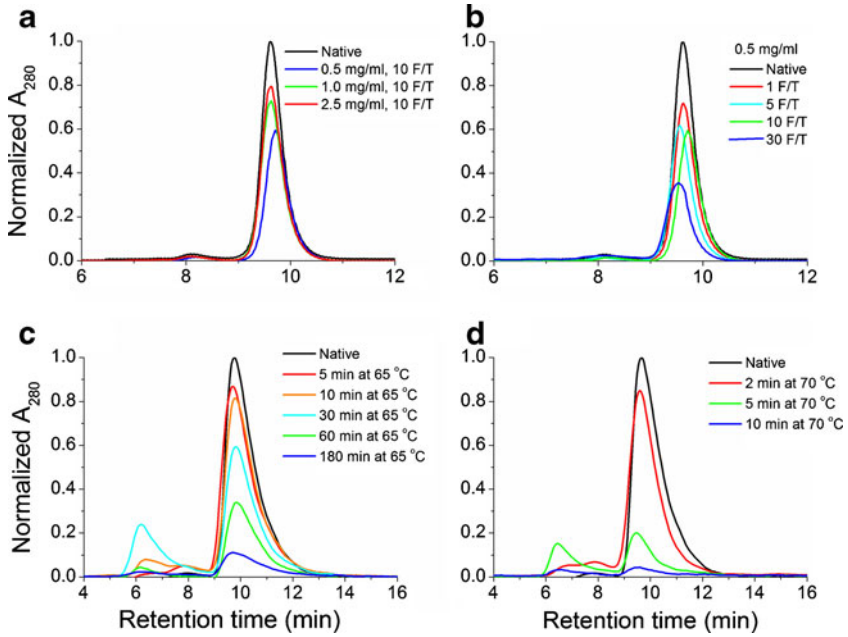

Fig. 2 HPSEC analysis of Bevacizumab aggregation induced by F/T and high temperature. (**a**) Effect of total protein concentration on the monomer eluted for samples treated with 10 F/T cycles. (**b**) Effect of number of F/T cycles on Bevacizumab aggregation for samples prepared at 0.5 mg/mL. (**c**, **d**) Aggregation under two incubation temperatures at 65 and 70°C, respectively. All the elution peaks are normalized to a control sample of native protein at the same concentration.

labeling patterns over the exchange time across the whole sequence. No significant difference in deuterium labeling was observed for any of the reporter peptides. This indicated that the LC in F/T-induced aggregates had molecular structure similar to that in the native state. Likewise, the HC HX patterns between native Bevacizumab and F/T-induced aggregates were generally quite similar, suggesting the HC of Bevacizumab F/T aggregates also had native-like structure. However, small but measurable increases in deuterium labeling (~10% or less) were observed for multiple reporter peptides, as shown in Fig. 4. The small differences suggest that the HC portion of the aggregates is largely native-like, but there may be a subtle conformational change occurring after F/T-induced aggregation.

Structure Analysis of Thermally Induced Bevacizumab Aggregates by HX-MS

Thermally induced Bevacizumab aggregates were also analyzed by peptide level HX-MS. Figure 5 compares the HX patterns of both LC and HC between native Bevacizumab and the aggregates formed by incubation at 70°C. In contrast to F/T-induced aggregates, the antibody aggregates formed by exposure to elevated temperature exhibited pronounced changes in HX patterns relative to the native state in both the LC and HC. Notably, both significant increases and decreases in deuterium labeling of the aggregates relative to native protein were observed in different parts of the antibody sequence. They are highlighted in red and blue ovals, respectively, in Fig. 5.

In the LC of Bevacizumab, dramatically increased deuterium labeling in thermally induced aggregates was observed in six different regions, as shown by the portions of primary sequence circled in red in Fig. 5a. The regions of increased labeling span ~50% of the LC, indicating that substantial unfolding occurred in the LC after aggregation induced by thermal stress. Conversely, only one short reporter peptide covering residues 48–54 showed decreased deuterium labeling in the aggregates relative to the native state. This reporter peptide was in the second complementarity determining region (CDR, sequence highlighted in red) in the LC. For the HC in Fig. 5b, increased deuterium labeling after thermally induced aggregation was also observed in six regions, while decreases in deuterium labeling were observed in two reporter peptides that were also located in the CDRs (residues 27–35 and 54–64). Interestingly, except the reporter peptide from the C-terminus at residues 430–452, all the other regions with pronounced changes in deuterium labeling for thermally induced aggregates are located in the variable domain V_H and the first constant domain CH1 (or the Fab portion) in the HC. In combination with the HX changes observed across the LC, the HX analysis suggested that most of the increases in conformational flexibility caused by thermally induced aggregation took place in the Fab fragment. On the other hand, three peptides within the CDRs (LC 48–54, HC 27–35 and HC 54–64) in the Fab fragment showed increased solvent protection after aggregation, indicating they might contribute to the intermolecular interactions responsible for antibody aggregation under thermal stress. Figure 6 shows the spatial distributions of regions of increased (red) and decreased (blue) deuterium labeling in aggregates relative to native antibody. From the figure, it is apparent that a majority of the regions with increased

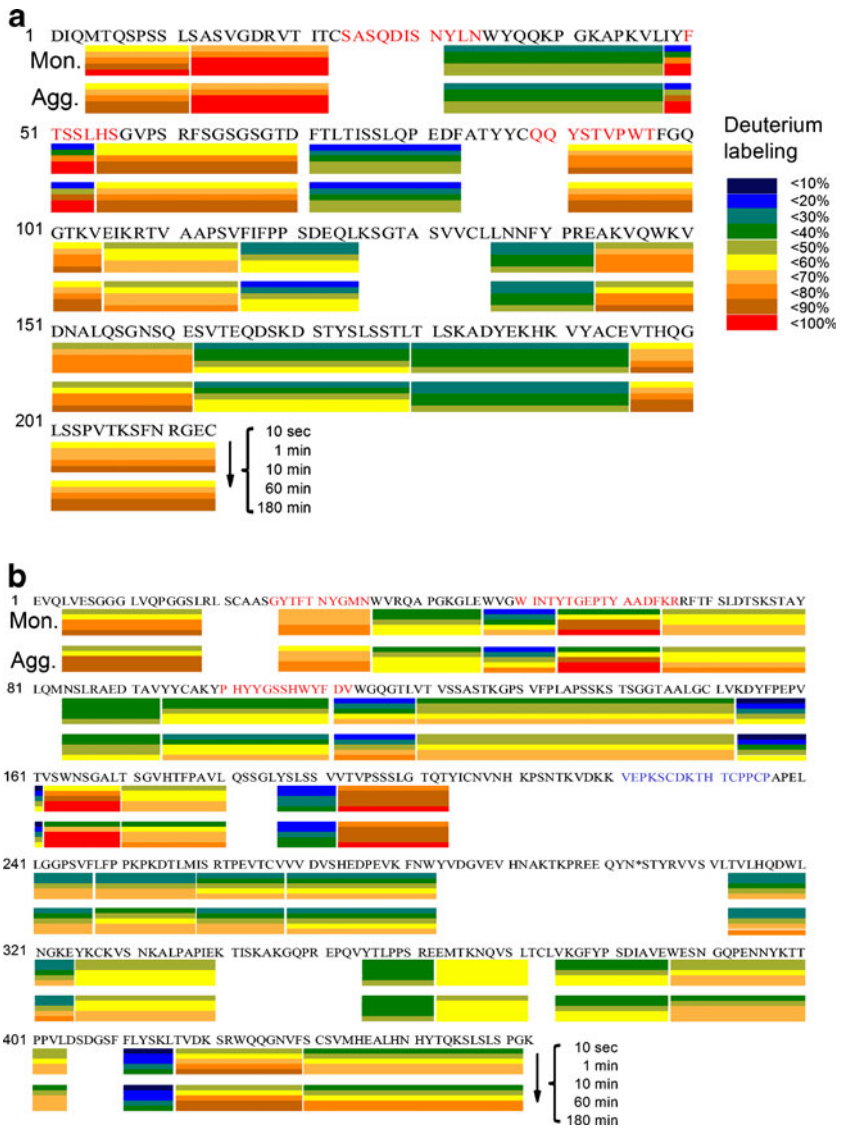

Fig. 3 Peptide level HX labeling patterns of LC (**a**) and HC (**b**) for native Bevacizumab and F/T induced aggregates. The labeling for each reporter peptide is shown by the two sets of five colored bars underneath the corresponding portion of the primary sequence. For each reporter peptide the labeling of native protein is shown by the top five bars, and the labeling of aggregates is shown by the bottom five bars. Each set of bars represents the labeling at five different labeling times (from top to bottom, 10 s, 1 min, 10 min, 60 min and 180 min). The percentage of deuterium labeling for each reporter peptide at each labeling time point is color coded using the scale shown in (**a**).

solvent accessibility after aggregation are located in the interface between the variable and constant domain in the Fab fragment.

Structure Comparison of Bevacizumab Aggregates by Fluorescence

As described above, peptide level HX analysis indicated that the two kinds of aggregates possess distinct monomer structures: native-like under F/T stress *vs.* an unfolded Fab domain under thermal stress. To further confirm this finding, intrinsic Trp fluorescence and extrinsic dye ANS binding measurements were performed. In Fig. 7a, intrinsic Trp fluorescence showed that the aggregates after 5 to 30 F/T cycles had no significant difference in the emission spectra relative to that of native sample, consistent with native-like HX patterns shown in Fig. 3. In contrast, the aggregate sample formed by incubation at 70°C for 10 min exhibited both red shift and dramatic signal increase in the emission spectrum, indicative of more unfolded structure in the aggregated state. Notably, the fluorescence signal associated with thermally induced aggregate sample was higher than the fully unfolded control in 6 M guanidine HCl.

Consistent results were also observed in the ANS binding assay, which is a measurement of solvent-exposed hydrophobic patches on protein surface (30). In Fig. 7b, native Bevacizumab and the aggregate samples after F/T cycles both had fluorescence spectra very similar to the ANS buffer, suggesting Bevacizumab molecules in two states were highly folded, precluding ANS binding. Conversely, the aggregate sample prepared at 70°C exhibited dramatically increased ANS binding, as suggested by the fluorescence signal increase as well as the significant blue shift. This result suggested that the thermally induced Bevacizumab

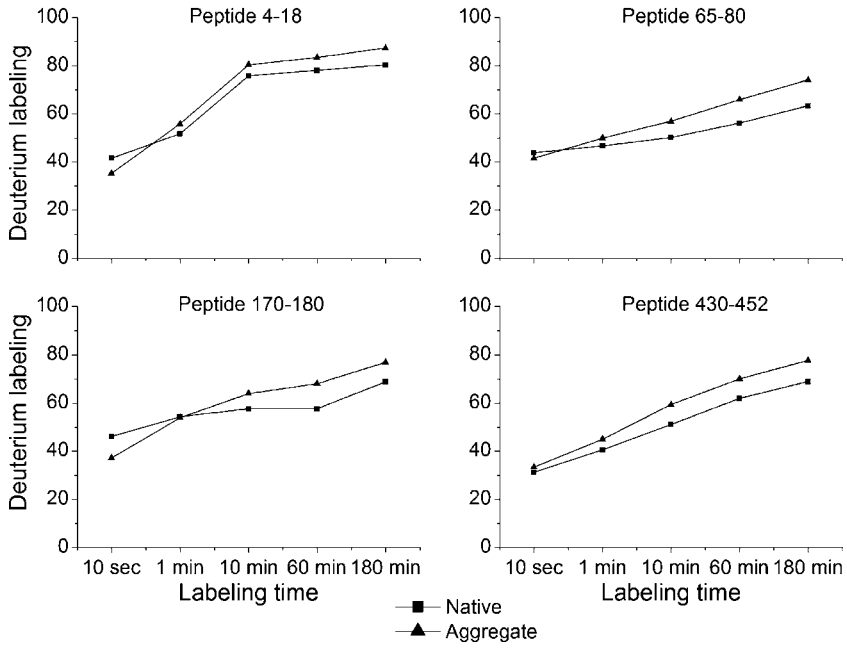

Fig. 4 Deuterium labeling of four representative reporter peptides *versus* labeling time for native Bevacizumab and F/T-induced aggregates.

aggregates were comprised of monomers with more unfolded structure relative to the native structure, consistent with HX analysis and Trp fluorescence measurements.

Aggregation-Prone Region Prediction by SAP Calculation

Prediction of aggregation-prone regions for monoclonal antibodies has been attempted from two computational approaches using sequenced-based calculators TANGO and PAGE (31) and simulation-based spatial aggregation propensity (SAP) analysis.(25) However, only the latter has been correlated with experiment by introducing mutations into predicted aggregation-prone regions to reduce antibody aggregation propensity (25). Here, we performed a similar SAP analysis as that described previously (25) to Bevacizumab to see if the reporter peptides with reduced HX labeling relative to native are predicted to be aggregation prone. SAP was defined and calculated as described in the Materials and Methods section. Figure 8 shows the residue-specific SAP profiles calculated for Bevacizumab LC, HC Fab and HC Fc in three panels, respectively. The SAP values were averaged over 8 data sets: two simulations for each of two starting structures modeled with antibody structures 1HZH and 1IGY, with each simulation generating two data sets for two identical chains. The bars below the SAP profile in each panel show the pattern of changes in local solvent protection after thermally induced aggregation. HX experiments showed three segments (LC 48–54, HC 27–35 and HC 54–64) with increased solvent protection in thermally induced aggregates relative to native state. Thus, these were considered as regions contributing to intermolecular contacts in Bevacizumab. The residue-averaged SAPs for these three segments are 0.040 (LC 48–54), 0.012 (HC 27–35) and −0.003 (HC 54–64). A two sample *t*-test using the statistical variance from the simulations was performed and suggested that the SAP values for the three aggregation forming segments are not statistically higher (i.e. more aggregation prone) than the rest of reporter peptides at the confidence level $p=0.05$. The result suggests that an SAP analysis as carried out in this study does not reliably predict the aggregation-forming segments within Bevacizumab. Although there is one small spike with SAP 0.140 at Leu54 of the LC, it is statistically indistinguishable from other similar or larger spikes in regions not experimentally implicated in intermolecular interations, and thus does not provide predictive ability in this situation. The major difference between the current SAP calculation and previous calculations is the use of an implicit rather than an explicit solvent model. However, the structural stability of the simulations performed in this study and the high statistical correlation between SAP calculated in this study and with the original SAP (see Figure S1) suggest that SAP calculated using the methods in this paper should be equivalent to previous SAP calculations at a qualitative level.

Aggregation-Prone Region Prediction by Sequence-Based Predictors

Algorithms predicting self-association based on primary sequence alone were also evaluated in terms of their ability to identify the residues exhibiting reduced solvent accessibility in the thermally induced aggregate. The consensus prediction of five different sequence-based methods,

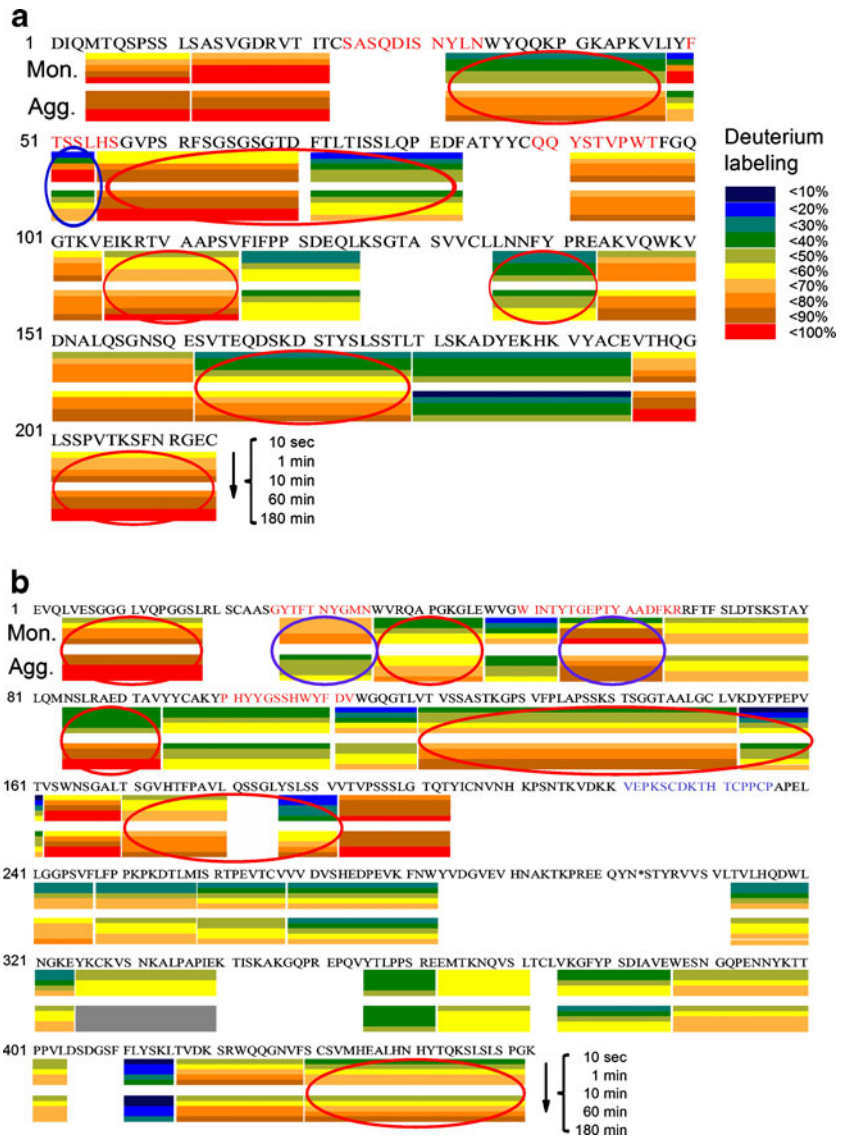

Fig. 5 Primary sequence representation of HX-MS labeling. Peptide level HX labeling patterns of LC (**a**) and HC (**b**) for native Bevacizumab and thermally induced aggregates. The labeling for each reporter peptide is shown by the two sets of five colored bars underneath the corresponding portion of the primary sequence. For each reporter peptide the labeling of native protein is shown by the top five bars, and the labeling of aggregates is shown by the bottom five bars. Each set of bars represents the labeling at five different labeling times (from top to bottom, 10 s, 1 min, 10 min, 60 min and 180 min). The percentage of deuterium labeling for each reporter peptide at each labeling time point is color coded using the scale shown (**a**). The regions with dramatic increased and decreased deuterium labeling after thermally induced aggregation are circled in red and blue, respectively. The gray block in (**b**) indicates the reporter peptide that was not detectable in the aggregate analysis.

AmylPred, was used for this purpose (32–36). The results are shown in the Supplementary Material (Tables S1 and S2). The stretches of primary sequence identified by four or five of the methods included light chain residues 46–50, 135–136 and heavy chain residues 281–285, 409–413. There was very little overlap between these residues and the observed segments within the antibody that had reduced solvent accessibility in the aggregates (LC 48–54, HC 27–35 and HC 54–64). Calculations of TANGO (32) and PAGE Z-score (8) identified a portion of the light chain segment, but only with the latter metric (Table S3).

DISCUSSION

mAb aggregation under different processing stresses represents a major challenge in therapeutic development. The distinct behaviors observed for different antibodies or different stressing conditions complicate the analysis of mechanism underlying antibody aggregation (1,7,11). Moreover, the detailed structural analysis of protein aggregates remains challenging because of their heterogeneous and disordered nature. In this study, HX-MS with proteolytic fragmentation was applied to characterize the molecular level structure of antibody aggregates formed under F/T and thermal stresses. By comparing the structural difference between native antibody and the monomers comprising two aggregates, distinct aggregation mechanisms were demonstrated for antibody Bevacizumab under F/T and high temperature aggregation conditions.

To our knowledge, this is the first application of HX-MS to analyze antibody aggregation. Although it is challenging to carry out HX-MS analysis with antibodies because of their large molecular size and numerous disulfide bonds, it

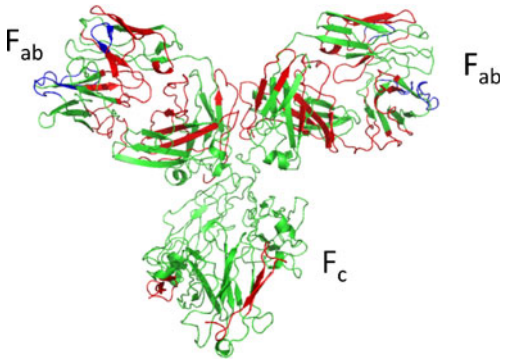

Fig. 6 Three-dimensional representation of regions of Bevacizumab showing significant increases and decreases in HX-MS labeling. The reporter peptides from Fig. 5 that showed significant increases (*red*) and decreases (*blue*) in deuterium labeling after thermally induced aggregation are indicated. The Bevacizumab structure was created by homology modeling using 1IGY as a template.

has recently been successfully accomplished for monomeric antibody conformation analysis in solution (37). In this study, we have developed new HX-MS procedures to analyze antibody structure perturbations upon freezing in the frozen state as well as monomer structure in the aggregated states after exposure to different stresses.

For antibody in the frozen state, the similar HX patterns between the sample of interest (in the absence of trehalose) and native control (in the presence of trehalose) suggested that Bevacizumab retained its native-like structure in the frozen state (Fig. 1). The structure integrity of Bevacizumab in the frozen state suggests that the antibody molecule was highly stable to the combined stresses introduced by the freezing process, such as low temperature, ice-solution interface, and freeze concentration of protein and solutes. This behavior differed from lactate dehydrogenase (LDH), a labile model protein for which a fraction of protein molecules became partially unfolded as suggested by increased deuterium labeling in HX-MS analysis upon freezing consistent with prior studies of LDH (29). Such a different behavior is also consistent with the higher conformational stability generally observed for antibody molecules relative to enzymes (38).

The high stability of Bevacizumab to freezing stress was further manifested with increasing chemical denaturant guanidine HCl in the frozen state. Up to ~2 M after freeze-induced concentration, Bevacizumab could still maintain its native-like structure in the LC. Interestingly, the HC was relatively more sensitive to the freezing stress than the LC and became partially denatured in the presence of Guanidine HCl as suggested by increased solvent accessibility in multiple local regions (Fig. 1b). These denatured regions (residues 3–18, 36–80, 248–268 and 430–452) presumably represent the local structure in Bevacizumab antibody that are least stable to the freezing stress. More interestingly, these unfolded regions were identified from different domains of the HC, rather than in one single domain. This pattern of unfolding observed in the frozen state contrasts to the pattern generally observed for antibody structure unfolding in solution which typically shows sequential unfolding of individual domains (30). This different pattern in unfolding may indicate distinct mechanisms causing antibody denaturation between the frozen and solution states.

Repeated F/T cycles induced Bevacizumab aggregation, the extent of which was influenced by protein concentration and F/T cycle number (Fig. 2a, b). The decrease in fraction of unfolded, aggregated protein with increasing protein concentration is consistent with the idea that as protein concentration increases, the fraction of protein required to cover the ice-water interface decreases. This observation has been made previously (29).

The fact that F/T cycling leads to oligomers that are stable to dilution and chromatography suggests that such oligomers may be composed of monomers with altered conformation. However, peptide level HX analysis of isolated aggregates showed that the F/T-induced antibody aggregates were made up of monomers exhibiting native-like deuterium exchange patterns (Fig. 3). Likewise, Trp fluorescence and ANS binding analysis also could not distinguish the structure of monomers in aggregates from

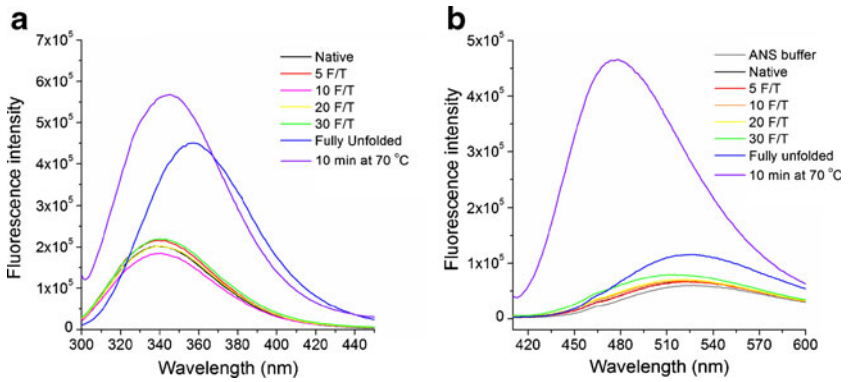

Fig. 7 Trp fluorescence (**a**) and ANS binding (**b**) of two Bevacizumab aggregates formed under F/T and thermal stresses.

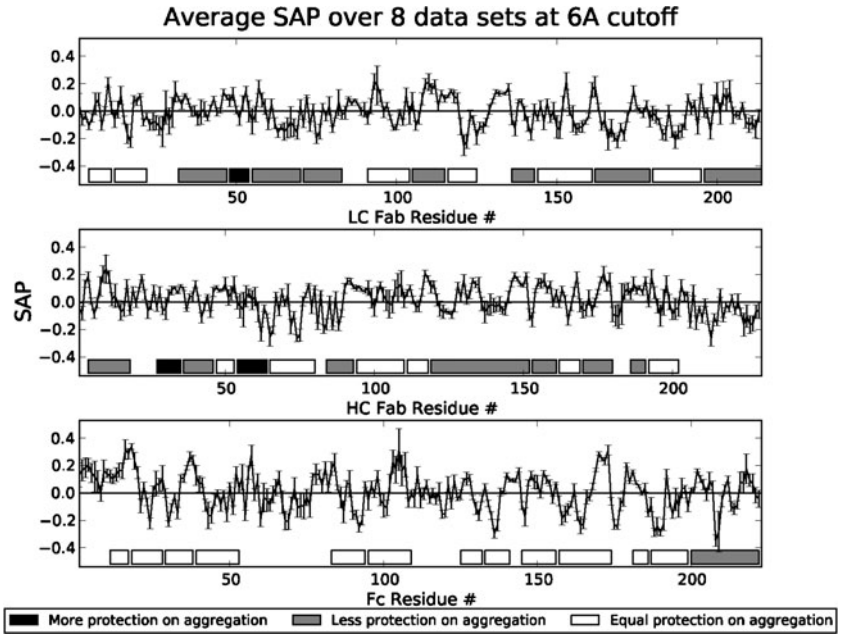

Fig. 8 Comparison of SAP aggregation-prone region prediction with peptide level HX measurement for Bevacizumab. The SAP value for each residue was averaged over eight data sets, four for each of two starting antibody structures modeled from 1HZH and 1IGY, respectively. The horizontal bars in each panel represent reporter peptides with changes in measured solvent protection by HX after thermally induced aggregation. Three reporter peptides exhibiting reduced labeling indicative of intermolecular contacts in aggregates are shown in black columns.

those under native conditions (Fig. 7). Thus, if conformational changes are involved, they must be subtle. This agreed with the high structure stability of antibody molecule against the freezing stress described above. In a previous study, we have also demonstrated that labile protein such as LDH with low structure stability to the freezing stress would accordingly produce non-native aggregates consisting of more unfolded monomers after F/T cycles (28). For antibody aggregation caused by F/T stress, similar conclusion has also been made for a different antibody in a different study (8), but the evidence was based on the analysis of global antibody structure by CD and FTIR.

As described above, F/T-induced antibody aggregates were made up of native-like monomers. However, subtle structural changes were also indicated associated with the aggregation by the small but detectable HX changes in some regions (Fig. 3), mainly with increases in local solvent accessibility for the aggregates relative to the native state. Interestingly, these HX increases were mainly found across the HC rather than the LC. This observation suggested that the subtle structural changes caused by Bevacizumab aggregation mainly occur to the HC, which might be consistent with the lower freezing stability observed for the HC described before (Fig. 1). Further, the subtle structural changes after Bevacizumab aggregation were found across the HC sequence instead of in a particular domain (Fig. 3), suggesting that the native molecule self-association may be mediated by intermolecular interactions occurring to all the HC domains, which is in contrast to the specific Fab-Fab interactions implicated in a previous study of native antibody self-association in highly concentrated formulation (9).

By contrast to F/T-induced aggregation, incubation at elevated temperature triggered non-native aggregation with the major substantial structural changes detected only in the Fab portion of Bevacizumab molecule by HX-MS (Fig. 5). Trp fluorescence and ANS binding, though only providing global structural information, suggested a more unfolded monomer structure in thermally induced aggregates (Fig. 7), consistent with the dramatic increases in local solvent accessibility in the Fab portion. It is also interesting to note that the HX patterns for the Fc portion were very similar between native Bevacizumab and the thermally induced aggregates except the C-terminal region 430–452. This observation suggested that the Fc fragment of antibody molecule retained its native-like structure; therefore, it may not be involved in the intermolecular interactions critical for protein aggregation. It should be noted that the experiments here cannot identify the details of the kinetic mechanism of the nonnative self-association that occurred. While aggregation may have occurred while the protein was held at elevated temperature, it is also possible that some of the structural perturbation was due to an inability to refold when the protein was returned to low temperature. Because the structural measurements were performed only after both heating and cooling steps, we cannot distinguish between these possibilities.

In Fig. 5, the substantial structure changes observed in the Fab fragment implicated its critical role during thermally induced aggregation. In previous studies, the Fab fragment has also been identified as the responsible domain for antibody aggregation under thermal stress. However, the employed experimental approaches were not based on the direct analysis of antibody aggregates; thus,

the conclusion regarding the responsible domain for antibody aggregation was not supported by direct and strong evidence. For example, Garber *et al.* concluded the critical role of the Fab fragment in aggregation based on the correlation between thermal stability of Fab fragment and molecular aggregation propensity for multiple antibodies under thermal stress (39). Other researchers identified the aggregation responsible domain based on the similarity of aggregation behavior between intact antibody and isolated fragments (7,8). By contrast, we demonstrated the critical role of Fab fragment in aggregation by illustrating the occurrence of substantial structural changes only to this portion for the thermally induced aggregates.

In thermally induced antibody aggregates, in addition to the major increases in the measured HX patterns, significantly decreased solvent accessibility (or increased solvent protection) was also observed in three short CDRs, LC 48–54, HC 27–35 and HC 54–64. Increase in local solvent protection relative to native state has been indicative of intermolecular contacts formed in protein-protein complexes and/or aggregates previously (18). Therefore, the three CDRs with more solvent protection in the antibody aggregates were believed to form intermolecular interactions responsible for Bevacizumab aggregation under high temperature. To our knowledge, this is the first time residues likely to be involved in antibody aggregate intermolecular contacts have been identified.

In pharmaceutical development, identifying the aggregation-prone regions in protein sequences could be of great interest, as it can provide the potential targets for protein engineering to enhance protein stability against processing stresses (25). However, to date, a well-established experimental approach that could effectively map the aggregation-forming regions from the given protein sequence has not been available. Computational predictions developed based on two general strategies utilizing either protein physicochemical properties (32) or molecular simulation (25) seem to be a promising method for this purpose. However, their accuracy in predicting the aggregation-prone regions has not been extensively tested by experiment, particularly for full-length large proteins such as monoclonal antibody (25). As demonstrated in this study, HX-MS can be a useful experimental tool to identify the regions forming intermolecular contacts in aggregates based on increased solvent protection relative to native monomer. It thus provides a method to test the ability of computational predictors. For the case of Bevacizumab, the combined use of two sequence-based aggregation calculators PAGE and TANGO suggested four short aggregation-prone regions in the LC and three in the HC (31), but none of them were coincident with LC 48–54, HC 27–35 and HC 54–64 that were identified by HX analysis in this study. Similar sequence-based calculations performed in this study showed little coincidence of predicted hot spots with regions of reduced solvent accessibility in the aggregates (Tables S1–S3). Similarly, in simulation-based SAP analysis, the three aggregation-forming segments were not predicted to be more aggregation prone relative to the other reporter peptides. The poor correlation between prediction and HX measurement suggested that neither the sequence-based calculators nor SAP could reliably predict the regions to form intermolecular contacts for antibody at least for our aggregation system.

In summary, we demonstrated the use of HX-MS as a new approach to explore the structural mechanism of antibody aggregation under two different stresses. In particular, Bevacizumab was shown to exhibit native aggregation under F/T stress *vs.* non-native aggregation under thermal stress. The high resolution associated with peptide level HX analysis further enabled identification of three polypeptide segments from CDRs as the likely regions to form intermolecular contacts during high temperature aggregation. HX-MS therefore provides valuable detailed structural information for biophysical analysis as well as potential input for protein engineering efforts to reduce aggregation.

ACKNOWLEDGMENTS & DISCLOSURES

The authors wish to thank Pfizer for financial support, as well as Karan Mehra (University of Virginia) for assistance with antibody simulations. This research was supported in part by the National Science Foundation through TeraGrid resources provided by NCSA Lincoln under grant number TG-MCB100015.

REFERENCES

1. Wang W, Singh S, Zeng DL, King K, Nema S. Antibody structure, instability, and formulation. J Pharm Sci. 2007;96(1):1–26.
2. Gabrielson JP, Brader ML, Pekar AH, Mathis KB, Winter G, Carpenter JF, *et al.* Quantitation of aggregate levels in a recombinant humanized monoclonal antibody formulation by size-exclusion chromatography, asymmetrical flow field flow fractionation, and sedimentation velocity. J Pharm Sci. 2007;96(2):268–79.
3. Shire SJ, Shahrokh Z, Liu J. Challenges in the development of high protein concentration formulations. J Pharm Sci. 2004;93(6):1390–402.
4. Purohit VS, Middaugh CR, Balasubramanian SV. Influence of aggregation on immunogenicity of recombinant human Factor VIII in hemophilia A mice. J Pharm Sci. 2006;95(2):358–71.
5. Rosenberg AS. Effects of protein aggregates: an immunologic perspective. AAPS J. 2006;8(3):E501–507.
6. Vermeer AW, Norde W. The thermal stability of immunoglobulin: unfolding and aggregation of a multi-domain protein. Biophys J. 2000;78(1):394–404.
7. Chen S, Lau H, Brodsky Y, Kleemann GR, Latypov RF. The use of native cation-exchange chromatography to study aggregation

and phase separation of monoclonal antibodies. Protein Sci. 2010;19(6):1191–204.
8. Hawe A, Kasper JC, Friess W, Jiskoot W. Structural properties of monoclonal antibody aggregates induced by freeze-thawing and thermal stress. Eur J Pharm Sci. 2009;38(2):79–87.
9. Kanai S, Liu J, Patapoff TW, Shire SJ. Reversible self-association of a concentrated monoclonal antibody solution mediated by Fab-Fab interaction that impacts solution viscosity. J Pharm Sci. 2008;97(10):4219–27.
10. Welfle K, Misselwitz R, Hausdorf G, Höhne W, Welfle H. Conformation, pH-induced conformational changes, and thermal unfolding of anti-p24 (HIV-1) monoclonal antibody CB4-1 and its Fab and Fc fragments. Biochim Biophys Acta. 1999;1431(1):120–31.
11. Van Buren N, Rehder D, Gadgil H, Matsumura M, Jacob J. Elucidation of two major aggregation pathways in an IgG2 antibody. J Pharm Sci. 2009;98(9):3013–30.
12. Hermeling S, Crommelin DJA, Schellekens H, Jiskoot W. Structure-immunogenicity relationships of therapeutic proteins. Pharm Res. 2004;21(6):897–903.
13. Griko YV, Privalov PL, Sturtevant JM, Venyaminov SYu. Cold denaturation of staphylococcal nuclease. Proc Natl Acad Sci USA. 1988;85(10):3343–7.
14. Chang BS, Kendrick BS, Carpenter JF. Surface-induced denaturation of proteins during freezing and its inhibition by surfactants. J Pharm Sci. 1996;85(12):1325–30.
15. Izutsu K, Yoshioka S, Terao T. Effect of mannitol crystallinity on the stabilization of enzymes during freeze-drying. Chem Pharm Bull. 1994;42(1):5–8.
16. Murase N, Franks F. Salt precipitation during the freeze-concentration of phosphate buffer solutions. Biophys Chem. 1989;34(3):293–300.
17. Smith DL, Deng Y, Zhang Z. Probing the non-covalent structure of proteins by amide hydrogen exchange and mass spectrometry. J Mass Spectrom. 1997;32(2):135–46.
18. Kheterpal I, Wetzel R. Hydrogen/deuterium exchange mass spectrometry–a window into amyloid structure. Acc Chem Res. 2006;39(9):584–93.
19. Vlcková M, Kalman F, Schwarz MA. Pharmaceutical applications of isoelectric focusing on microchip with imaged UV detection. J Chromatogr A. 2008;1181(1–2):145–52.
20. Friedrichs MS, Eastman P, Vaidyanathan V, Houston M, Legrand S, Beberg AL, *et al.* Accelerating molecular dynamic simulation on graphics processing units. J Comput Chem. 2009;30(6):864–72.
21. Hornak V, Abel R, Okur A, Strockbine B, Roitberg A, Simmerling C. Comparison of multiple Amber force fields and development of improved protein backbone parameters. Proteins. 2006;65(3):712–25.
22. Bashford D, Case DA. Generalized born models of macromolecular solvation effects. Annu Rev Phys Chem. 2000;51:129–52.
23. Ryckaert J-P, Ciccotti G, Berendsen HJC. Numerical-integration of cartesian equations of motion of a system with constraints—molecular-dynamics of N-alkanes. J Comput Phys. 1977;23:327–41.
24. Chennamsetty N, Helk B, Voynov V, Kayser V, Trout BL. Aggregation-prone motifs in human immunoglobulin G. J Mol Biol. 2009;391(2):404–13.
25. Chennamsetty N, Voynov V, Kayser V, Helk B, Trout BL. Design of therapeutic proteins with enhanced stability. Proc Natl Acad Sci USA. 2009;106(29):11937–42.
26. Fraternali F, Cavallo L. Parameter optimized surfaces (POPS): analysis of key interactions and conformational changes in the ribosome. Nucleic Acids Res. 2002;30(13):2950–60.
27. Göller K, Ofer A, Galinski EA. Construction and characterization of an NaCl-sensitive mutant of Halomonas elongata impaired in ectoine biosynthesis. FEMS Microbiol Lett. 1998;161(2):293–300.
28. Zhang A, Qi W, Singh SK, Fernandez EJ. A new approach to explore the impact of freeze-thaw cycling on protein structure: hydrogen/deuterium exchange mass spectrometry (HX-MS). Pharm Res. 2011;28(5):1179–93.
29. Strambini GB, Gabellieri E. Proteins in frozen solutions: evidence of ice-induced partial unfolding. Biophys J. 1996;70(2):971–6.
30. Ionescu RM, Vlasak J, Price C, Kirchmeier M. Contribution of variable domains to the stability of humanized IgG1 monoclonal antibodies. J Pharm Sci. 2008;97(4):1414–26.
31. Wang X, Das TK, Singh SK, Kumar S. Potential aggregation prone regions in biotherapeutics: a survey of commercial monoclonal antibodies. MAbs. 2009;1(3):254–67.
32. Fernandez-Escamilla A-M, Rousseau F, Schymkowitz J, Serrano L. Prediction of sequence-dependent and mutational effects on the aggregation of peptides and proteins. Nat Biotechnol. 2004;22(10):1302–6.
33. Galzitskaya OV, Garbuzynskiy SO, Lobanov MY. Prediction of amyloidogenic and disordered regions in protein chains. PLoS Comput Biol. 2006;2(12):e177.
34. Hamodrakas SJ, Liappa C, Iconomidou VA. Consensus prediction of amyloidogenic determinants in amyloid fibril-forming proteins. Int J Biol Macromol. 2007;41(3):295–300.
35. López dela Paz M, Serrano L. Sequence determinants of amyloid fibril formation. Proc Natl Acad Sci USA. 2004;101(1):87–92.
36. Zhang Z, Chen H, Lai L. Identification of amyloid fibril-forming segments based on structure and residue-based statistical potential. Bioinformatics. 2007;23(17):2218–25.
37. Houde D, Arndt J, Domeier W, Berkowitz S, Engen JR. Characterization of IgG1 conformation and conformational dynamics by hydrogen/deuterium exchange mass spectrometry. Anal Chem. 2009;81(7):2644–51.
38. Manning MC, Chou DK, Murphy BM, Payne RW, Katayama DS. Stability of protein pharmaceuticals: an update. Pharm Res. 2010;27(4):544–75.
39. Garber E, Demarest SJ. A broad range of Fab stabilities within a host of therapeutic IgGs. Biochem. Biophys Res Commun. 2007;355(3):751–7.